Compression experiments with spin-polarized atomic hydrogen

R. Sprik and J. T. M. Walraven

Natuurkundig Laboratorium, Universiteit van Amsterdam, Valckenierstraat 65, 1018 XE Amsterdam, The Netherlands

Isaac F. Silvera

Lyman Laboratory of Physics, Harvard University, Cambridge, Massachusetts 02138
(Received 13 May 1985)

Doubly polarized hydrogen has been produced up to densities of 2×10^{18} cm^{-3} with the use of a compression technique. Samples were compressed up to five orders of magnitude into small bubble-like volumes under a column of liquid helium. This technique enabled us to study the volume decay of a bubble at almost constant gas density for minutes. The analysis of the volume decay of such a bubble is discussed. A bulk three-body recombination process was observed with rate constant $C_3 = [7(2)] \times 10^{-39}$ cm^{6}s^{-1}, as well as bulk electronic $b \rightarrow c$ relaxation with rate constant $G_{bc}^v \downarrow = [12(4)] \times 10^{-16}$ cm^{3}s^{-1}. The nature of the three-body process is analyzed with a set of extended rate equations. The samples were very delicate and rapid compressions could result in explosions.

I. INTRODUCTION

In the rapidly developing field of spin-polarized atomic hydrogen (H↓), one of the principal experimental goals is to achieve high densities of H↓ at low temperatures.[1-3] Under these conditions many-body effects and phenomena of quantum degeneracy of the gas become important. Hydrogen in its atomic form is a composite boson consisting of an electron (spin $S = \frac{1}{2}$) and a proton (spin $I = \frac{1}{2}$). A gas of H↓ is believed to behave as a weakly interacting Bose gas and one expects the system to undergo a phase transition to a Bose-Einstein condensed (BEC) state, possibly exhibiting superfluid behavior.[4] For example, to observe the transition at $T_c = 100$ mK, the gas has to be stabilized to densities $n = 1.6 \times 10^{19}$ cm^{-3} ($T_c = 3.31 \hbar^2 n^{2/3} / m K_B$).

In this paper we report on experiments in which we have extended the experimentally accessible density regime by an order of magnitude to $n = 2 \times 10^{18}$ cm^{-3}. A short report of this work was published earlier.[5] Hess et al.[6-8] developed a different technique for the same purpose and achieved densities $n \simeq 4.5 \times 10^{18}$ cm^{-3}. At these high densities one observes interesting new phenomena such as three-body recombination, spontaneous explosion of gas samples, and relaxation to electron spin-reversed states. However, the densities are not sufficiently high or the temperature sufficiently low to observe BEC. Before we discuss the specific aspects of our experiment, we briefly review the conditions that enable manipulation of H at high densities.

In its atomic form H is unstable against recombination to the $^1\Sigma_g^+$ electronic singlet state of the hydrogen molecule. Experimentally, recombination is suppressed by electron-spin polarizing the gas (H↓) with a strong magnetic field, forcing the atoms to interact pairwise via the nonbinding "triplet" potential associated with the $^3\Sigma_u^+$ electronic state of the H-H system. An important aspect in stabilizing H↓ is that the recombination not only has to

be suppressed in the bulk, but also for atoms adsorbed on the walls of the sample cell. This is done by coating the walls of the cell with liquid helium which has a very low binding energy (ε_a) for H atoms (e.g., for ^{4}He, $\varepsilon_a / k_B \simeq 1$ K). Therefore at moderately low temperatures the surface density of H atoms, which depends exponentially on $\varepsilon_a / k_B T$, remains relatively low and the recombination on the surface is suppressed.

The electronic-spin polarization of the gas and the related stability is limited by the presence of the hyperfine interaction. The "well-known" hyperfine level diagram of hydrogen in a magnetic field is shown in Fig. 1. The two lower states $|a\rangle = -|\downarrow \Uparrow\rangle + \varepsilon |\uparrow \Downarrow\rangle$ and $|b\rangle = |\downarrow \Downarrow\rangle$ are the spin states occupied in an H↓ sample. Here ↓ and ⇓ denote the electron- and proton-spin projections, respectively, and $\varepsilon = a / 4\mu_B B$ is the hyperfine mixing coefficients; a is the hyperfine coupling constant, and μ_B is the Bohr magneton. The upper states, $|c\rangle = |\uparrow \Downarrow\rangle + \varepsilon |\downarrow \Uparrow\rangle$ and $|d\rangle = |\uparrow \Uparrow\rangle$, are thermally depopulated at low temperature. Due to the hyperfine coupling between proton and electron spin, $a \mathbf{I} \cdot \mathbf{S}$, there is an intrinsic difference in recombination probability between atoms in the a state and the b state. The a state atoms have a small admixture (ε) of electron spin-up, limiting the electronic polarization to $1 - \varepsilon^2$ and giving rise to singlet behavior during collisions with other atoms. Atoms in the b state are in a "pure," fully-polarized Zeeman state. Consequently a-state atoms have a higher probability to recombine than atoms in the b state, leading to a faster depletion of the a state than the b state and to a gas of predominantly b-state atoms: nuclear and electron-spin ("doubly") polarized hydrogen (H↓⇓).[9,10] Historically the decay of H↓⇓ was first attributed[9,10] to a magnetic relaxation mechanism[10-13] and more recently to dipolar recombination.[6,7,14,15,13] Remarkably, many properties that are known for H↓ were obtained by studying the density decay due to recombination, showing that although recombination is detrimental if one aims at the highest densities,
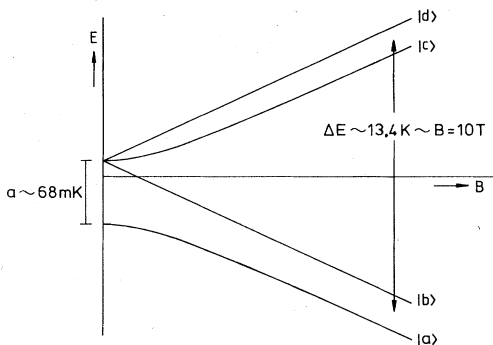
FIG. 1. Hyperfine level diagram of a hydrogen atom in a magnetic field B.

it in fact facilitates the study of many of the properties of H↓.

In earlier experiments H↓ was fed into a sample cell until a steady state was achieved between filling flux and the dominant decay process. In this way H↓↑ has been produced at densities up to $3 \times 10^{17} \text{cm}^{-3}$ and estimated polarizations of 99.9%.[10,11] When the filling stage is terminated, the decay of the density is observed, using a convenient probe, ranging from calorimetric tools in the early days of H↓ experiments to sophisticated resonance probes to observe the NMR and ESR in the gas.[16,1,2,3] One of the intrinsic difficulties with such an approach is that the gas density decays fastest in the interesting high-density regime, so that high densities are observable only during the very short initial period, just after terminating the filling procedure when uncertainties about thermal equilibrium are largest.

In this paper we expand our earlier report[5] on experiments in which we maintain the system under nominally constant pressure conditions while the effects of recombination are studied by observing the decay of the sample volume. This novel approach enables us to observe the system during periods of minutes at densities 10 times higher than previously possible for periods of seconds. In these experiments a gas of H↓↑ is compressed to densities up to $2 \times 10^{18} \text{ cm}^{-3}$; new destabilization processes are observed which will be discussed in the following sections. Other compression experiments in which H↓↑ was studied up to densities $n \simeq 4.5 \times 10^{18} \text{ cm}^{-3}$ were done at the Massachusetts Institute of Technology (M.I.T.).[6,7,14,15,8] Apart form a large overlap with our results, these measurements also provide information on surface related phenomena.

II. EXPERIMENTAL APPARATUS

Before describing the details of the sample cell used in the present measurements, we give a short general description of the experimental configuration.

A. General cryogenic system

The experiments are carried out in an Oxford Instruments (1000-μmole/s circulation) dilution refrigerator with access from the bottom (Fig. 2). The sample cell is

placed in the center of a 11-T superconducting magnet (Thor Cryogenics, 2.5-cm bore), which creates a parabolic field profile in the cell region.[17] The cell is thermally connected to the mixing chamber by a 1.5-cm-diam. copper rod. The atoms are fed into the cell from the bottom and are produced in a room temperature H_2-discharge operated at 2.45 GHz.[18] The discharge pressure is stabilized to 1—2 Torr using a simple gas handling system with a zeolite-filled cold trap at liquid-N_2 temperature, which purifies the hydrogen and provides a buffer of H_2 gas. The gas handling system is also used to introduce helium into the cell. After dissociation the atoms flow through a constriction in the discharge tube into a teflon-covered 6-mm-diam. transport tube.[18] Before it enters the cryostat the gas passes through a teflon valve, which enables us to isolate the cryogenic part from the rest of the system. The atoms are cooled down in a few stages by heat ex-
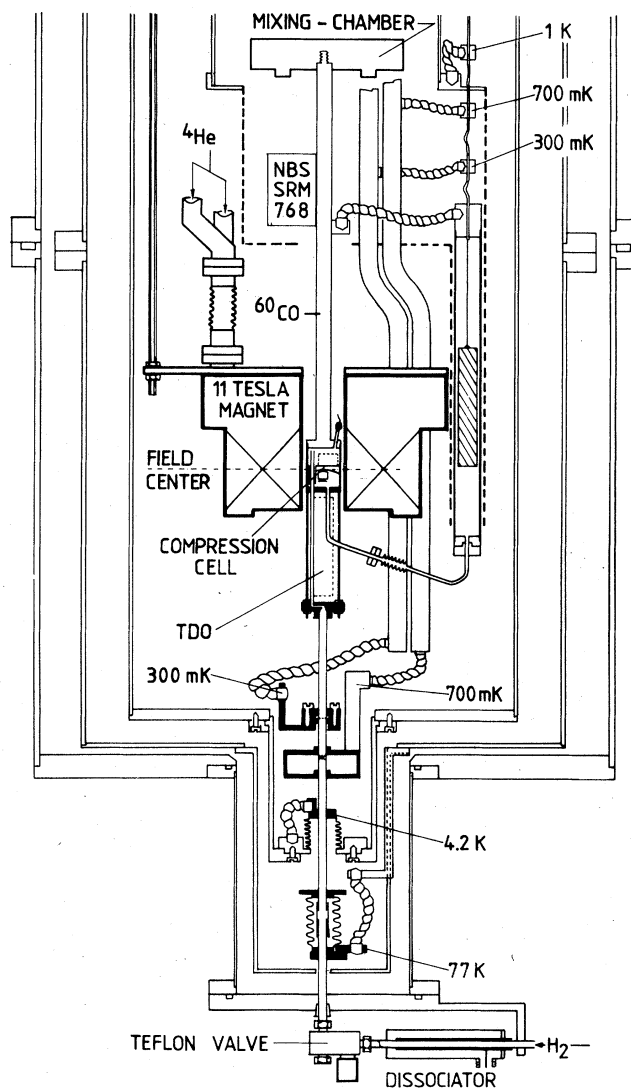

FIG. 2. Schematic diagram of the H↓↑ compression experiment in a ^{3}He-^{4}He dilution refrigerator.

change with the walls of the filling line (see Fig. 2) as has been described elsewhere.[1,18] Thermal pinning points for this purpose are derived from intermediate temperature available in the dilution refrigerator. The a- and b-state atoms are localized in the high-field region by magnetic compression.[17]

B. Compression cell

The general arrangment of our compression cell is shown in Fig. 3. The heart of the cell, located inside of the magnet bore, is separated into two chambers, the upper part (UP) and the lower part (LP) which are connected by tubes extending almost to the bottom of the LP. Entering the bottom of the cell are two tubes: the H↓ fill tube and a tube leading to a large liquid-helium reservoir outside of the magnet. Due to a U-tube arrangement, the helium is distributed over the inner and outer chambers.

The gas may be compressed by up to 5 orders of magnitude in four stages. With the helium level low (stage 1), H↓ fed into the cell fills both the UP and LP to a density of about 10^{15} cm^{-3}. By lowering a large copper block in the outer leg (OL), the He level rises until it seals the bottom of the tubes connecting the UP and LP, isolating the LP region ($\simeq 1.5$ cm^3, stage 2). Then the helium level is gradually (in about 1 min) raised by lowering the block further, compressing the gas to smaller volumes (stage 3), in which an equilibrium of the polarization is achieved (see Sec. IV C). Eventually (stage 4) the hydrogen is compressed into a small "bubblelike" volume ($V \geq 2 \times 10^{-3}$ mm^3) completely immersed in the liquid at the curved top of the LP and is detected by a volume gauge. Since the helium level is above the bubble, there is a hydrostatic pressure on the bubble proportional to the helium column head (1 mm He at $T < 1$ K$\simeq 1.42$ Pa$\simeq 10^{-2}$ Torr). The recombination of atoms results in the decay of the volume of the bubble under nearly constant hydrostatic pressure.

The volume of the bubble of compressed H↓↑ is measured with a capacitance gauge. The capacity reaches its maximum value when the gauge is completely filled with liquid helium. The capacitance change due to displacing He with a bubble of H↓↑($\varepsilon = \varepsilon_0$) is a direct measure of the sample volume. Calibration of the volume gauge is done by measuring the relative change in capacitance when filling an empty gauge completely with helium. This gives $\Delta C/C = (1 - \varepsilon_r)/\varepsilon_r (\Delta V/V)$ ($\varepsilon_r = 1.057$ for pure ^{4}He at temperatures < 1 K).[19] The volume of the gauge is 17.7 mm^3 and $\Delta V = 6.59 \times 10^{-4}$ pF/mm^3. The resolution is approximately 10^{-3} mm^3.

The helium level is detected by a coaxial capacitance level gauge, based on the same principle as the volume gauge. Inside the cell, on top of the volume gauge we mounted a resistance thermometer (Matsushita, 200Ω, covered with 1266 Stycast epoxy) to measure the temperature of the plate. These three devices make it possible to follow the decay of the volume under a known hydrostatic pressure and a known ambient temperature. Furthermore, the system includes a membrane-pressure gauge for vapor-pressure thermometry and to monitor the loading of the cell with hydrogen, as well as a trigger bolometer[20] to enable complete removal of the sample.

The construction of the volume gauge is sketched in more detail in Fig. 4(a). It consists of the measuring capacitance (plates $A-B$, 0.9 mm apart and 6 mm wide, radius of curvature 10 mm), a reference capacitance (plates $B-C$) and a guard ring D. The difference in capacitance between $A-B$ and $B-C$ is measured with a General Radio 1615A capacitance bridge. This scheme compensates for temperature effects, etc. The plates of the volume gauge are covered with 200-mm^3 silver sinter (0.1-μm grain size) to minimize Kapitza resistance between the helium and the plates. The sinter is filled with liquid helium through capillary action and cannot be penetrated by the H↓↑ gas. Since plates A, B, and C have to be electrically floating, the removal of the heat from these plates is somewhat indirect. The heat of recombination once coupled to the liquid, is extracted via plates A and B and via a small gap filled with liquid helium towards a sinter covered part of the body of the cell (D). The heat exchange between the H↓↑ gas and the helium will be discussed in Sec. IV D.

The level gauge is shown in more detail in Fig. 4(b). The capacitance of this gauge is measured with a capacitance to frequency conversion technique.[21] The coaxial capacitor is the frequency determining element in the LC
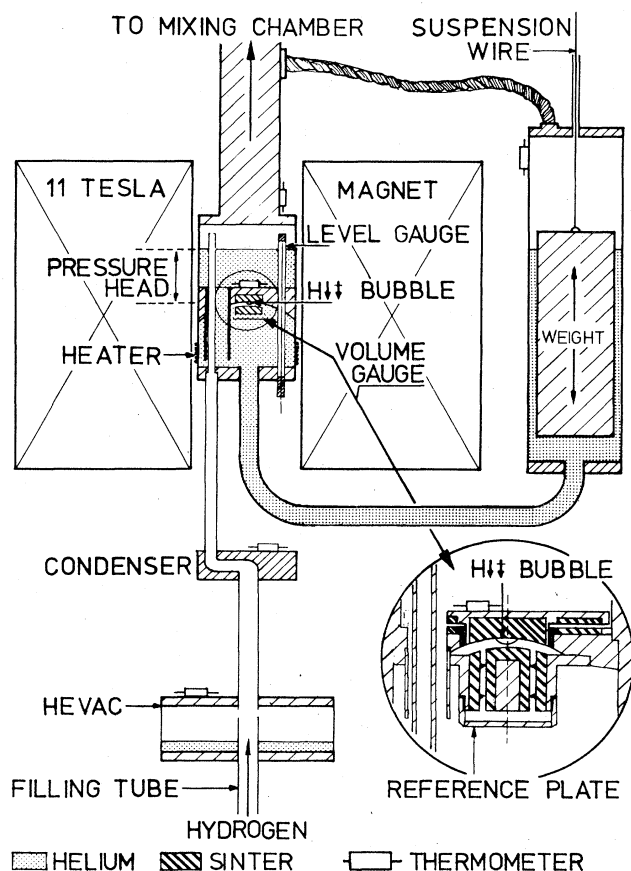

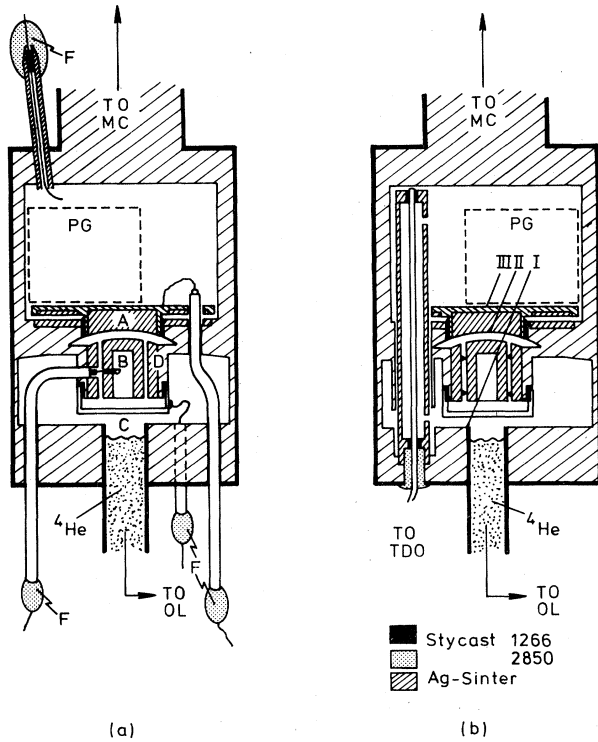FIG. 3. H↓↑-compression cell (schematic).

FIG. 4. Detailed cross section of the compression cell inside the magnet. (a) Volume gauge. (b) Level gauge. PG represents pressure gauge, F represents electrical feedthrough, TDO represents tunnel-diode oscillator, and MC represents mixing chamber. The ^{4}He tube connects to the outer leg (OL) of the cell. The H↓ filling line is not shown in this drawing; it would require a third cross section

circuit of a tunnel diode oscillator (TDO) operating at 10.6 MHz. The coil, the tunnel diode (General Electric backward diode BD6) and a feedback capacitor are directly mounted under the cell (see Fig. 2); bias resistors are placed on a 1-K post nearby. The calibration of the level gauge is fixed by determining the frequency when the helium is at the lowest point in the cell [level I, Fig. 4(b)] and at the point just above the volume gauge (level III). The location of these points is determined by inducing U-tube oscillations, sweeping the helium level across levels I and III. The change in cross section at I and III shows up as a change in oscillation amplitude. Using ^{4}He, oscillations are easily generated with a small periodically varying temperature gradient between the legs. The varying fountain pressure then leads to the oscillations. Using the known distance between I and III [12.4(2) mm] and the distance between III and the top of the volume gauge [level II, 2.8(3) mm], the zero column height level is determined and also the sensitivity (about 2.3 kHz/mm He with a resolution of 10^{-2}mm). This calibration had to be done for each field setting, due to a slight field dependence of the characteristics of the tunnel-diode circuit ($\simeq$0.4 kHz/T).

The column height measured this way is not directly

proportional to the applied pressure on the bubble. An additional effect is caused by the gradients in our parabolic magnetic field. Due to the diamagnetic susceptibility of ^{4}He, the column tends to be pushed out from the magnet and thus gravity is partially compensated. One can easily show that in the parabolic field the overall resulting pressure at the field center is[22]

$$p_k = p_{\text{gravity}} + p_{\text{diamagnetic}}$$
$$= \rho g z + \tfrac{1}{2}(X_m/\mu_0)[B^2(x,z) - B^2(0,0)]$$

with

$$B^2(x,z) = B_0^2 \{ [1 - (z/z_m)^2 + \tfrac{1}{2}(x/z_m)^2]^2 + (xz/z_m^2)^2 \},$$

where X_m is the diamagnetic susceptibility of liquid helium $(X_m = 8.7 \times 10^{-7})$,[23] $\mu_0 = 4\pi \times 10^{-7}$ Hm^{-1} is the permeability of vacuum, and x,z is the radial position and height of the helium meniscus. For our magnet $z_m = 5.1 \times 10^{-2}$ m. This effect is especially important when z becomes large (e.g., for $B_0 = 10$ T, $r = 0$, and $h = 10$ mm the pressure is reduced to 75% of the value in a homogeneous field).

In an earlier paper[5] these diamagnetic effects on the column pressure were not taken into account. Therefore our present value for the third-order coefficient C_3 is substantially larger than in Ref. 5 and in better agreement with the results of Hess *et al.*[6,7] Note that the same diamagnetic effect also causes a difference in level positions between the cell part inside and outside the magnet.

Level oscillations can also be used to study the compressibility of H↓↑ gas. The pressure (Δp) and volume (ΔV) variations associated with the oscillations may be measured with the level and volume gauge, respectively, and should be related through the compressibility κ: $\Delta V/V = \kappa \Delta p$. One expects κ to be isothermal [$\kappa_T = -1/V(\partial V/\partial p)_T = 1/p$ for an ideal classical gas] as long as the heat contact between the H gas and the liquid helium is good. In the absence of thermal contact, κ is the adiabatic compressibility [$\kappa_S = -(1/V)(\partial V/\partial p)_S = \tfrac{3}{5}(1/p)$ for an ideal monatomic classical gas]. Also a stepwise change of p gives information on the compressibility. This method may ultimately lend itself to the observation of BEC where a factor of 2 change in κ_T is predicted at T_c.[3]

C. Thermometry

To measure the temperature of the various parts in the cell, several carbon resistance thermometers were used (Fig. 3). Although most of these thermometers were previously calibrated, a numer of calibration devices were also mounted on the cell to check the calibration. For the low-temperature regime ($T = 20-300$ mK) the calibration was done in zero-field against a National Bureau of Standards (NBS) fixed-points device (SRM 768) and a ^{60}Co nuclear orientation thermometer. For the regime at $T = 300-900$ mK the calibration was done against the ^{3}He and ^{4}He vapor pressures, making use of the internal pressure gauge and an external gauge (Barocel 1173) to measure the vapor pressure. The resistance thermometers are field dependent and must be calibrated *in situ* for each

magnetic field setting. Since the nuclear orientation thermometer and the fixed-points device are no longer useful once the field has been turned on, the calibration in field is done by transferring the zero-field calibration to the higher fields by cycling the field up and down. The calibration reproduced within 2% of previous ones.

III. ANALYSIS OF THE VOLUME DECAY

To analyze our data we use a simple rate equation to describe the decrease of the total number of particles N in a doubly polarized gas:

$$dN/dt = -F(n)N , \qquad (3.1)$$

where $F(n)$ is a polynomial in the density n. Under the appropriate conditions the polynomial coefficients may be compared with decay coefficients provided by theory (see Sec. IV C). For instance, allowing only for two-body $b \rightarrow a$ volume relaxation (rate constant G_{ba}^v which bottlenecks rapid a-b recombination) and three-body volume recombination (rate constant K_{bbb}^v) one may write

$$F(n) = C_2 n + C_3 n^2 , \qquad (3.2)$$

where $C_2 = 2G_{ba}^v$ and $C_3 = 2K_{bbb}^v$.

Using the ideal gas law, $pV = Nk_B T$, gives for the decay rate under isothermal condition:

$$\tau^{-1} \equiv \dot{V}/V = -F(n)[1 + (V/p)dp/dV]^{-1} . \qquad (3.3)$$

In general the gas pressure $p = p_k + p_\gamma$ is the sum of the pressures due to the helium column height, p_k, measured with respect to the top of the bubble and corrected for the diamagnetic susceptibility of helium p_{diam} and a bubble volume and shape-dependent part p_γ. The latter term $p_\gamma \equiv p_\alpha + p_\beta$ has a contribution due to the surface tension of the liquid-helium surface, p_α, and the buoyancy pressure, $p_\beta = \Delta\rho g h$, where $\Delta\rho$ is the difference in mass density between liquid and gas, g is the acceleration of gravity, and h is the height of the bubble (see Fig. 5). p_γ increases during the decay of the volume.

Before addressing ourselves to the case of a nonspherical bubble at arbitrary pressure, we first consider two important limiting regimes for the volume decay; the isobaric regime and the surface tension dominated regime. In the isobaric regime p is predominantly determined by the hydrostatic pressure head ($p_k \gg p_\gamma$) and the volume decay rate (τ^{-1}) is constant:
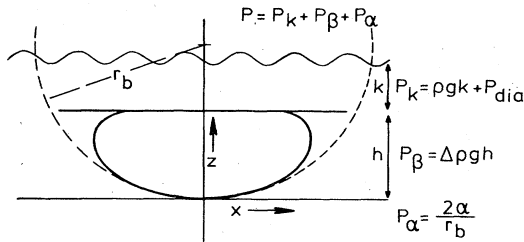

FIG. 5. Definition of symbols used in calculation of the shape of a sessile bubble. The column pressure p_k is also influenced by the gradient in the magnetic field (p_{diam}, see the text).

$$\tau^{-1} = -F(p_k/k_B T) . \qquad (3.4a)$$

Hence, the volume decays exponentially:

$$V(t) = V_0 \exp(-F[p_k/k_B T]t) . \qquad (3.4b)$$

This regime is characteristic for most of our experiments with bubbles in the 0.5—2.0 mm^3 range. A typical decay for this regime is illustrated in Fig. 6.

For small bubbles the buoyant forces are negligible ($p_\beta \ll p_\alpha$) so that the bubble is spherical. Then $p_\gamma \simeq p_\alpha = 2\alpha/r \equiv \hat{a}/V^{1/3}$,[24] where r is the radius of the bubble, α the surface tension of helium and $\hat{a} = 2\alpha(4\pi/3)^{1/3}$ (for ^{4}He at $T < 1.2$ K; $\alpha = 3.7 \times 10^{-4}$ Nm^{-1}).[25] Hence Eq. (3.3) reduces to

$$\tau^{-1} = -F(p/k_B T)[p/(p - \tfrac{1}{3}p_\alpha)] , \qquad (3.5)$$

with $p = p_k + p_\alpha$. Furthermore, if $p_k \ll p_\alpha$, which holds for very small bubbles, surface tension effects are dominant and τ^{-1} becomes

$$\tau^{-1} = -\tfrac{3}{2} F(p_\alpha/k_B T) . \qquad (3.6)$$

The transition to the surface tension dominated regime is illustrated in Fig. 7 for a bubble under small applied pressure where the decay is approximately second order in nature and τ^{-1} approaches a $V^{-1/3}$-like behavior. One notes that even at 10^{-2} mm^3 the observed decay still deviates from a decline according to Eq. (3.6).

An accurate relation between p_γ and V, taking into account the detailed shape of the bubble, may be derived starting from the Young and Laplace equation for the surface pressure of a curved surface:[24]

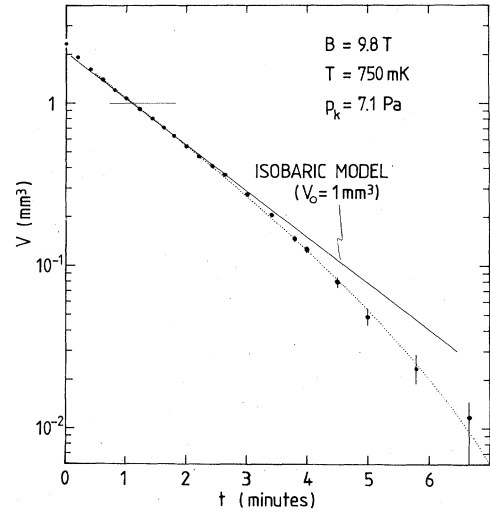$$\alpha(1/R_1 + 1/R_2) = p - p_l(x,z) . \qquad (3.7a)$$

FIG. 6. Example of a decay at relatively high column pressure ($p_\gamma \ll p_k$). The solid line represents the exponential approximation for an isobaric decay, the dotted line is the fit of the decay using the calculated pressure p_γ. For $V > 1.4$ mm^3 the volume gauge is no longer linear.
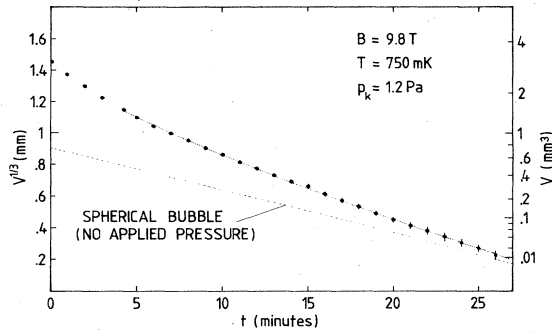
FIG. 7. Example of a decay at relatively low column pressure $(p_\gamma \gg p_k)$. The dashed line represents an approximation with $p_k = 0$ and p_γ the surface tension of a spherical bubble, the dotted line is the fit of the decay using the calculated pressure p_γ. For $V > 1.4$ mm^3 the volume gauge is no longer linear.

Here R_1 and R_2 are the local radii of curvature of the bubble surface, p is the gas pressure in the bubble, and p_l is the pressure in the liquid at the evaluation point (x,z). The result of the model is illustrated in Fig. 5. We show the bubble deformed by the buoyant forces, which push the bubble against a flat plate. The contact angle between bubble and plate is zero, the limit of complete wetting of the surface. To describe the bubble shape we choose the x,z coordinate system with the origin at the lower apex of the bubble. At the origin, where $R_1 = R_2 \equiv r_b$, Eq. (3.7a) reduces to

$$p = p_l(0,0) + 2\alpha/r_b \equiv p_k + p_\gamma . \tag{3.7b}$$

Combining Eqs. (3.7a) and (3.7b) and using $p_l(0,0) - p_l(x,z) = \Delta\rho g z$ one finds

$$\alpha(1/R_1 + 1/R_2) = \Delta\rho g z + 2\alpha/r_b . \tag{3.7c}$$

In principle, the shape of the bubble depends on the presence of magnetic field gradients, but these effects are negligible since the bubble is very small and located in the center of the magnetic field. Exploiting the axial symmetry of the bubble with respect to the z axis one finds from differential geometry for R_1 and R_2:[24]

$$1/R_1 = \ddot{z}(1 + \dot{z}^2)^{-3/2} \tag{3.8a}$$

and

$$1/R_2 = \dot{z}[x(1 + \dot{z}^2)^{1/2}]^{-1} , \tag{3.8b}$$

where R_1 is the radius of curvature of the meridian,

$$\dot{z} \equiv (dz/dx) \equiv \tan(\Phi)$$

and

$$\ddot{z} \equiv d^2z/dx^2 \equiv \cos^{-2}(\Phi)(d\Phi/dx) .$$

The bubble problem may be reformulated in terms of a set of differential equations in x,z as a function of Φ which may be solved numerically once the curvature r_b at the apex is chosen:

$$dx^*/d\Phi = \cos(\Phi)/f(x^*,z^*) , \tag{3.9a}$$

$$dz^*/d\Phi = \sin(\Phi)/f(x^*,z^*) , \tag{3.9b}$$

where $x^* \equiv x/r_b$, $z^* \equiv z/r_b$, and

$$f(x^*,z^*) = [\Delta\rho g/(\alpha r_b^2)]z^* + 2 - \sin(\Phi)/x^* . \tag{3.9c}$$

The required relation between p_γ and V, taking into account the bubble shape, then follows from a numerical integration procedure. The results of the calculation for the case of ^{4}He are illustrated in Fig. 8. These are slightly different when using a curved top surface of the bubble instead of the flat top shown in Fig. 5. For the curvature used in the experiment, the difference between the results for a flat top and the actual curved top are less than 2%. The bubble model only applies for $V < 1.4$ mm^3, beyond which the bubble contacts both capacitor plates.

In principle, information on the second-order and third-order decay coefficients can be derived from one volume decay curve, provided p_k, T and B are known, with the use of this bubble model. The dotted lines in Figs 6 and 7 are fits to the data, obtained by numerical integration of Eq. (3.3) for an optimum choice of C_2 and C_3. The fit demonstrates that the bubble model enables
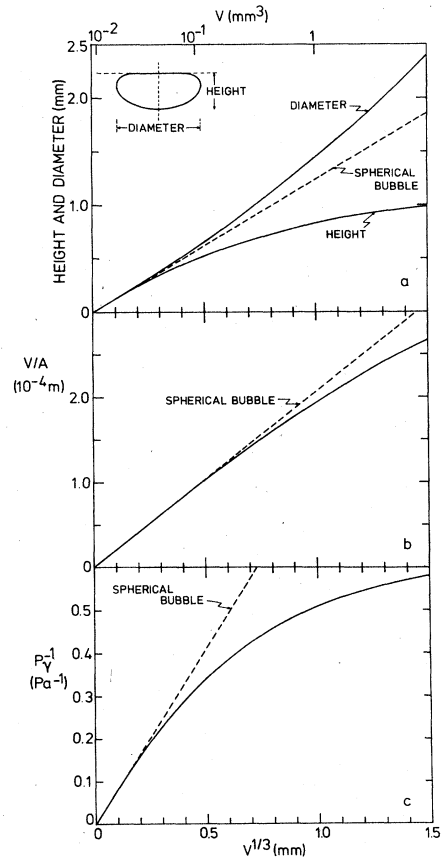

FIG. 8. Calculated properties of a sessile bubble in ^{4}He $(\alpha = 3.7 \times 10^{-4}$ Nm). Dashed line is a spherical bubble approximation.

an accurate description of the decay. However, the results depend very critically on the exactness of the bubble model and furthermore one neglects the influence of a changing A/V ratio on the coefficients C_2 and C_3. A more attractive approach, which is less sensitive to this problem, involves the combination of decay curves obtained for different p_k. This is done by measuring $\tau^{-1} \equiv \dot{V}/V$ at one specific volume V_0 (e.g., 1 mm^3) for different decay curves. The additional pressure $p_{\gamma 0} \equiv p_\gamma(V = V_0)$ and its volume derivative $(dp_\gamma/dV)_{V = V_0}$ are then the same for each density curve, independent of the exact shape of the bubble as long as this shape reproduces for each temperature and magnetic field. With the use of Eq. (3.3), τ^{-1} is

$$\tau^{-1} = -F[(p_k + p_{\gamma 0})/k_B T]/\mathscr{C}_{cor}(V_0) , \qquad (3.10)$$

with

$$\mathscr{C}_{cor}(V_0) = 1 + [V_0/(p_k + p_{\gamma 0})](dp_\gamma/dV)_{V = V_0} .$$

All corrections due to the change of the pressure as function of the volume are contained in the factor $\mathscr{C}_{cor}$. This factor is close to unity as long as $p_k > p_{\gamma 0}$, which is the case for our $V_0 = 1$-mm^3 data, as illustrated in Fig. 9.

The analysis of our experimental data is presented in Sec. IV and was done by measuring τ^{-1} at $V_0 = 1$ mm^3 in the volume decays for different values of p_k. Using the correction factor $\mathscr{C}_{cor}$ and $p_{\gamma 0}$ for $V_0 = 1$ mm^3, $\tau^{-1} \times \mathscr{C}_{cor}$, and $p = p_k + p_{\gamma 0}$ were obtained. Fitting $\tau^{-1}\mathscr{C}_{cor}$ versus p to a second-order polynomial through the origin gives the coefficients C_2 and C_3 in $F(p)$. To illustrate the consistency of the model for p_γ, Fig. 10 shows the data at 9.8 T and 750 mK analyzed for different volumes and combined in one plot. For the range of volumes considered (0.02—1.0 mm^3), p_γ changes about 4 Pa and the data points follow approximately a common parabola, although at small volumes (dotted line) a systematic deviation from the curve is observed in a detailed analysis. In Sec. IV C we will show that the deviation can be explained by the effect of a changing A/V ratio and its influence on the effective surface decay rates.
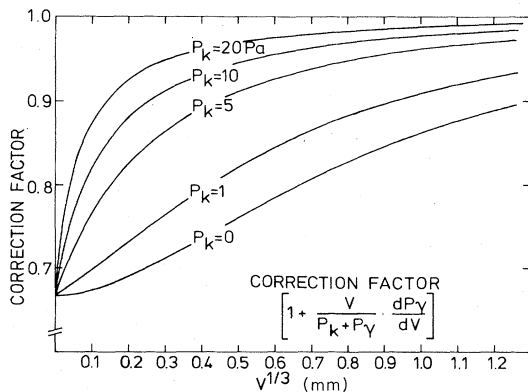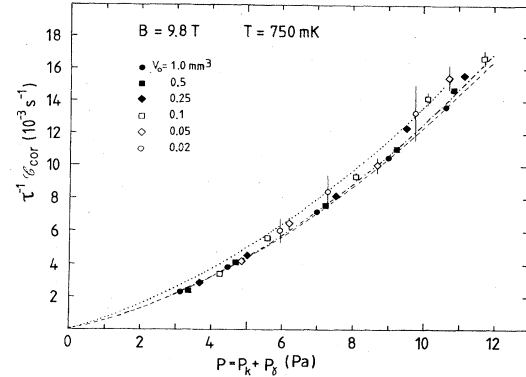

FIG. 10. Five decays at $B = 9.8$ T and $T = 750$ mK analyzed for different volumes V_0. The dashed line is a second-order fit to $V_0 = 1$ mm^3. The dashed-dotted line is a curve based on Eqs. (4.9) using the decay-rate constant from Table I. The dotted line idem but for $V_0 = 0.02$ mm^3 ($A/V = 150$ cm^{-1}). The deviation between the dashed-dotted and dotted line is attributed to the difference in the A/V ratio.

IV. RESULTS

A. General features

The highest pressure we could apply, using the compression scheme of Sec. II B, corresponds to $\simeq 12$-mm helium column ($\simeq 15$ Pa at 8 T) as limited by the dimensions of the sample cell. At the lowest ambient temperatures employed in this experiment ($T \simeq 700$ mK, using ^{4}He as compression fluid) this implies a density of $n \simeq 2 \times 10^{18}$ cm^{-3}. The assumption of thermal equilibrium will be discussed in Sec. IV D. The highest densities were achieved in bubbles with a volume $V = \simeq 0.1$ mm^3 and in an 8 T magnetic field.

High densities could only be obtained by compressing the sample at a relatively slow rate ($\simeq 1$ min) to the final pressures. Too rapid a compression was found to lead to a short (< 1 s) transient phenomenon in which the bubble disappeared after a sudden increase in volume (by as much as a factor of 10). These transients were accompanied by small spikes on the level gauge and on the internal thermometer of the cell, and were interpreted as the occurrence of an explosion in the gas. The explosions could always be induced by compressing sufficiently fast, even when the gas was carefully precompressed (stage 3, see Sec. II B) to induce double polarization. In a typical experiment we observed the decay of the volume over at least 1 order of magnitude from $\simeq 2$ mm^3 to 0.1 mm^3. This process was quite slow, especially at low densities, requiring termination of the decay by rapid compression to obtain a "zero-volume" reference measurement (Fig. 11). An attractive aspect of the explosions is that they enabled us to do such a zero-volume measurement at will, when useful. In this sense the explosions replace the use of the "trigger bolometer" in pressure decay measurements.

Under appropriate conditions ($B/T < 10$ T/K) the explosions were observed to occur "spontaneously" (Fig. 12). This is associated [5,26] with a new destabilization process that we identified: electronic dipolar ($b \rightarrow c$) relaxation

FIG. 9. Correction factor $\mathscr{C}_{cor}$ as a function of column pressure p_k and volume $V^{1/3}$ [Eq. (3.10)].
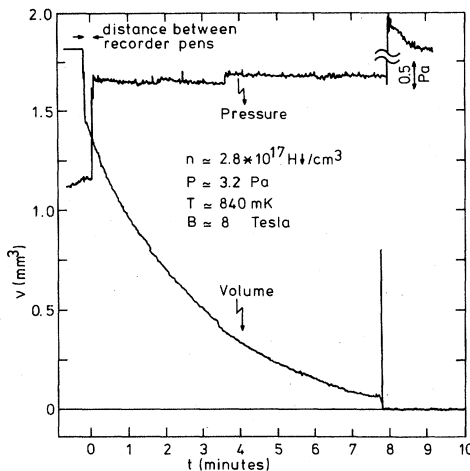
FIG. 11. Typical volume decay terminated by rapid compression, inducing an "explosion" of the gas.

which will be discussed in more detail in Sec. IV C. Recently, the explosions have been studied in more detail by Tommila et al.[27]

Perhaps the most significant result of the quantitative analysis of the decay curves was evidence for a third-order decay process with rate constant $C_3 = [7(2)] \times 10^{-39} \text{cm}^6$ s^{-1} ($B = 9.8$ T, $T = 750$ mK) and in good agreement with the result of Hess et al.[6,7] This process represents a very important barrier for obtaining high-gas densities since the decay rate is proportional to the cube of the density.

Although a quantitative analysis will only be given for the ⁴He case, we also obtained some results ³He/⁴He mixtures as compression fluid. Due to a cryogenic problem we could not measure below 650 mK with ⁴He liquid in the cell. Apparently the film flow of the superfluid helium out of the cell, and the back-fluxing helium vapor gave rise to an excessive heat load (estimated to be $\simeq 2$ mW). With a small admixture of ³He (1%) this problem was suppressed and the cell could be cooled below 100 mK.

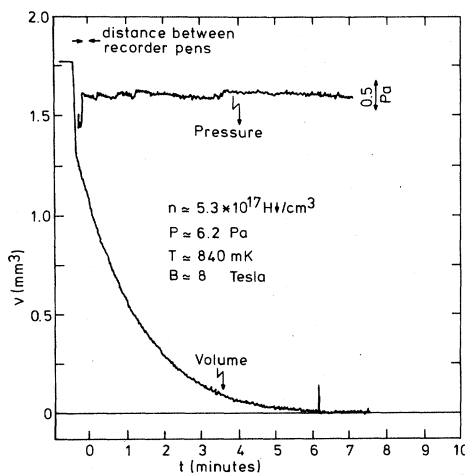The reported data on ⁴He cover the 650—900 mK temperature regime, where destabilization processes in the bulk gas dominate the surface processes. As such, this temperature regime is well suited to study the bulk destabilization processes of the sample. Compression data for ³He/⁴He mixtures were observed for temperatures ranging from 300—500 mK. Under those conditions the H↓ samples turned out to be much more susceptible to explosions than when using ⁴He as a compression fluid. Although we could produce densities of the same order of magnitude as in the ⁴He case, irreproducibilities in the data, which were likely due to poor thermal equilibrium, caused us to focus on the ⁴He data.

B. Analysis of the decay rates

We used the procedure in Sec. III to analyze the observed rate of change of the volume (τ^{-1}) as function of pressure, taking into account the correction factor $\mathscr{C}_{\text{cor}}$, p_γ, and the influence of the diamagnetic correction of p_k. In Fig. 13 we show $(1/p)\tau^{-1} \times \mathscr{C}_{\text{cor}}(V_0 = 1 \text{ mm}^3)$ versus p for magnetic fields $B = 9.8, 9, 8, 7$, and 6 T obtained for a temperature of $\simeq 710$ mK. The lines in Fig. 13 are fits of $\tau^{-1} \times \mathscr{C}_{\text{cor}}$ versus p to a second-order polynomial through the origin, where $(C_2/k_B T)$ is the intercept and $[C_3/(k_B T)^2]$ the slope [see Eqs. (3.2) and (3.10)]. For some fields the number of data points and the dynamic range of the density was quite limited (due to a rapidly decaying sample). The results for the field dependence of the second-order coefficient (C_2) are presented in Fig. 14(a), and for the third-order coefficient (C_3) in Fig. 14(b).

The results for the temperature dependence of the rates $(1/p)\tau^{-1} \times \mathscr{C}_{\text{cor}}$ versus p at $B = 8$ T are shown in Fig. 15. For 680 and 840 mK reliable data for C_2 and C_3 could be obtained. For 733 and 925 mK only one decay was recorded, which is not enough to deduce C_2 and C_3 independently. These data will be used only for an estimate of C_2, correcting for C_3, resulting in relatively large error bars.

C. Discussion of the decay results

To interpret our results, we consider the known recombination and relaxation processes in doubly polarized gas $(n_b \gg n_a)$ where the a state is depleted due to preferential
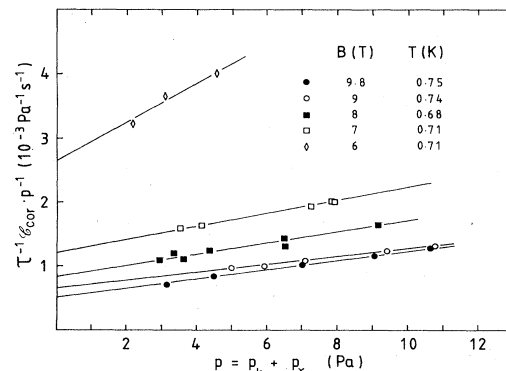

FIG. 12. Typical volume decay terminated by a spontaneous "explosion."

FIG. 13. Field dependence of the decay rates at $\simeq 710$ mK. The lines are fits to the data for different fields.
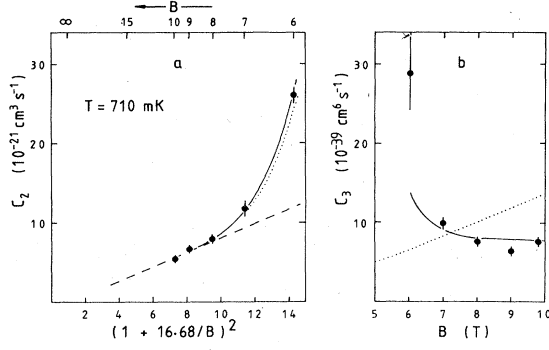
FIG. 14. Field dependence of (a) second-order (C_2) and (b) third-order (C_3) decay rates. (a) The dashed line is the contribution of volume relaxation: $G_{ba}^v T^{-1/2}(1+16.68/B)^{-2}$ $=6.9(6)\times10^{-22}$ cm^{3}s^{-1}. The solid line is the sum of G_{ab}^v and $G_{bc}^v \uparrow$ contribution (see text). Dotted line idem, but with $G_{bc}^v \downarrow$ the value obtained by Lagendijk et al. (Ref. 36). (b) The dotted line is the calculated volume recombination rate K_{bbb}^v (Ref. 29) multiplied by $2\theta_b=3.27$. The solid line is a fit to the data with $K_{bbb}^v=2.0(5)\times10^{-39}$ cm^{6}s^{-1} and $K_{bbc}^v=3(1)\times10^{-33}$ cm^{6}s^{-1} (see text).

recombination.[6] As our experiments were done at relatively high temperatures and/or low magnetic fields, we also considered the occupation of the c and d levels. In that case the evolution of the system is described by a set of four coupled rate equations. For simplicity we only retain the leading terms, assuming $n_d \ll n_c \ll n_a < ,n_b$. As we will discuss later, the degree of double polarization may not be sufficiently high to neglect all processes where two or more a-state atoms participate. The rate equations are

$$\dot{A}/V = -K_{ab}^{\mathrm{eff}}ab + G_{ba}^v(a+b)(b-a)+G_E^{\mathrm{eff}}(bd-ac)$$
$$\qquad -K_{abb}^{vv}ab^2 ,$$

$$\dot{B}/V = -K_{ab}^{\mathrm{eff}}ab - G_{ba}^v(a+b)(b-a)-G_E^{\mathrm{eff}}(bd-ac)$$
$$\qquad -K_{bc}^{\mathrm{eff}}bc - G_{bc}^v\uparrow(b+c)b + G_{bc}^v\downarrow(b+c)c$$
$$\qquad -K_{bd}^{\mathrm{eff}}bd -(2+\xi)K_{bbb}^v b^3 -K_{bbc}^v b^2c -K_{abb}^v ab^2 , \qquad (4.1)$$

$$\dot{C}/V = -K_{bc}^{\mathrm{eff}}bc - G_{bc}^v\downarrow(b+c)c +G_{bc}^v\uparrow(b+c)b$$
$$\qquad +G_E^{\mathrm{eff}}(bd-ac)+\xi K_{bbb}^v b^3 -K_{bbc}^v b^2c ,$$

$$\dot{D}/V = -K_{bd}^{\mathrm{eff}}bd -G_E^{\mathrm{eff}}(bd-ac) .$$

Adding all terms yields

$$\dot{N}/V = -2(K_{ab}^{\mathrm{eff}}ab +K_{bc}^{\mathrm{eff}}bc +K_{bd}^{\mathrm{eff}}bd$$
$$\qquad +K_{abb}^v ab^2+K_{bbb}^v b^3+K_{bbc}^v b^2c) .$$

Here capital letters represent numbers of particles and lower case letters represent number densities in a specific hyperfine level. The contributing rate constants at higher temperatures can be grouped in four classes. (a) The second-order rates K_{ab}^{eff}, K_{bc}^{eff}, etc., correspond to three-body recombination processes where a third body other than hydrogen enables conservation of energy and

momentum. Helium atoms of the helium surface can provide this third body for H atoms adsorbed on the helium film (K_{ab}^s). These surface processes are proportional to the surface coverage and hence exponentially dependent on the binding enregy (ε_a) of an H atom to the surface. At higher temperatures, where the helium vapor pressure becomes appreciable, the third body can also be a helium atom from the vapor $[K_{ab}^v(n_{\mathrm{He}})]$. Both bulk and surface processes are included in $K_{ab}^{\mathrm{eff}},K_{bc}^{\mathrm{eff}}$, etc.:

$$K_{ab}^{\mathrm{eff}}=(A/V)K_{ab}^s[\lambda_{th}\exp(\varepsilon_a/k_BT)]^2+K_{ab}^v(n_{\mathrm{He}})$$

with

$$\lambda_{th} =(2\pi\hbar^2/mk_BT)^{-1/2} .$$

(b) G_{ba}^v describes the two-body nuclear dipole-dipole relaxation in the bulk and $G_{bc}^v\uparrow$, $G_{bc}^v\downarrow$ the electronic dipolar relaxation. The ratio of $G_{bc}^v\uparrow$ and $G_{bc}^v\downarrow$ is determined by the Boltzmann factor:

$$G_{bc}^v\uparrow/G_{bc}^v\downarrow =\exp(-2\mu B/k_BT)\simeq\exp(-1.35B/T) .$$

Surface relaxation can be ignored at high temperatures. (c) G_E^{eff} relates to the spin-exchange process between a,c and b,d levels. All other spin-exchange processes are suppressed in high magnetic fields. Spin-exchange tends to maintain $a/b=d/c$. (d) K_{bbb}^v, K_{abb}^v, and K_{bbc}^v describe three-body hydrogen recombination processes in the bulk. K_{bbc}^v yields the recombination rate with one of the atoms in the c state. It is driven by the exchange recombination mechanism described by Kagan et al.[28] Similarly K_{abb}^v is associated with the exchange recombination with one of the atoms in the a state. Note that we introduced K_{abb}^v and K_{bbc}^v in the equations in spite of the fact that the only available theory for exchange recombination by Kagan et al.[28] implies $K_{abb}^v=\varepsilon^2K_{bbc}^v=0$ for $T\rightarrow0$. K_{bbb}^v is the three-body dipolar-recombination rate.[28] For each K_{bbb}^v event, a hydrogen molecule and an atom in the c state [fraction $\xi=0.91$ (Ref. 29)] or in the b state (fraction $1-\xi$) is produced. This c-state atom can relax to the b state $(G_{bc}^v\downarrow)$ or recombine either on the surface (K_{bc}^s) or in the gas phase (K_{bbc}^v).[15] In the latter two cases one event of K_{bbb}^v finally results in the production of two molecules
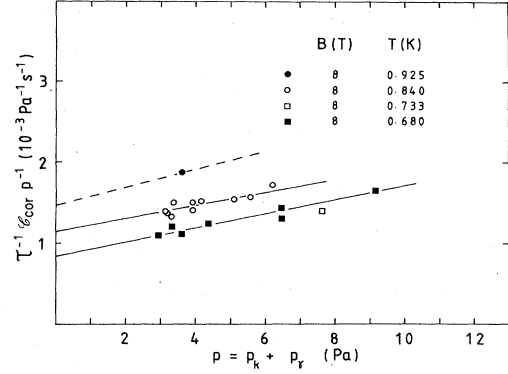

FIG. 15. Temperature dependence of the decay rates at $B=8$ T. For $T=733$ mK and $T=925$ mK only one data point is available. Dashed lines are fits to the data.

and a total loss of four b-state atoms. In the former case, only two atoms disappear from the b state. The dominant scenario is determined by the temperature, field and density conditions. Again surface three-body effects are ignored because at higher temperatures the surface coverage is too low.

To illustrate some features of this set of rate equations, assume that the density is sufficiently low to exclude third-order processes and that the temperature and/or field conditions are such ($B/T < 10$ T/K) that the c level is partially populated, while $n_d \ll n_c \ll n_b$ due to preferential recombination and spin-exchange. Then, Eqs. (4.1) reduce to

$$\dot{A}/(Vb^2) = -K_{ab}^{\text{eff}}\hat{a} + G_{ba}^v(1-\hat{a}^2) + G_E^{\text{eff}}(\hat{d} - \hat{a}\,\hat{c}) \ ,$$

$$\dot{B}/(Vb^2) = -K_{ab}^{\text{eff}}\hat{a} - G_{ba}^v(1-\hat{a}^2) - G_E^{\text{eff}}(\hat{d} - \hat{a}\hat{c})$$
$$\qquad -K_{bc}^{\text{eff}}\hat{c} + G_{bc}^v\!\downarrow(1+\hat{c})\hat{c} - G_{ab}^v\!\uparrow(1+\hat{c}) - K_{bd}^{\text{eff}}\hat{d} \ ,$$
$$\tag{4.2}$$

$$\dot{C}/(Vb^2) = -K_{bc}^{\text{eff}}\hat{c} - G_{bc}^v\!\downarrow(1+\hat{c})\hat{c} + G_{bv}^v\!\uparrow(1+\hat{c})$$
$$\qquad + G_E^{\text{eff}}(\hat{d} - \hat{a}\hat{c}) \ ,$$

$$\dot{D}/(Vb^2) = -K_{bd}^{\text{eff}}\hat{d} - G_E^{\text{eff}}(\hat{d} - \hat{a}\hat{c}) \ ,$$

with $\hat{a} \equiv a/b$, $\hat{c} \equiv c/b$, and $\hat{d} \equiv d/b$.

For the doubly polarized gas $\hat{a}$, $\hat{c}$, and $\hat{d}$ go to well-defined limit values for $t \to \infty$, $\hat{a}_0$, $\hat{c}_0$, and $\hat{d}_0$, which are independent of the history of the sample. Retaining only terms up to first order in $\hat{a}$, $\hat{c}$, and $\hat{d}$, this results in ratios

$$\hat{a}_0 = G_{ba}^v/(K_{ab}^{\text{eff}} - G_{bc}^v\!\uparrow) \ ,$$

$$\hat{c}_0 = G_{bc}^v\!\uparrow/(K_{bc}^{\text{eff}} + G_{bc}^v\!\downarrow) \ ,$$
$$\tag{4.3}$$

and $\hat{d}_0 = 0$. These relations are obtained by setting $\dot{\hat{a}}$, $\dot{\hat{c}}$, and $\dot{\hat{d}}$ equal to zero. Here $\hat{a}_0$ is a measure for the double polarization in the gas [the polarization is usually defined as $(b-a)/(b+a) = (1-\hat{a})/(1+\hat{a})$]. The ratio $\hat{c}_0$ expresses the competition between the relaxation of b-

state atoms to the c-state atoms ($G_{bc}^v\!\uparrow$) and the subsequent recombination (K_{bc}^{eff}) or relaxing back ($G_{bc}^v\!\downarrow$) of this c-state atom. Which process is dominant depends on temperature and on the geometry of the cell. If the recombination is much slower than the relaxation ($K_{bc}^{\text{eff}} \ll G_{bc}^v\!\downarrow$), $\hat{c}_0$ equals the ratio of the b and c level in thermal equilibrium. In the other limit ($K_{bc}^{\text{eff}} \gg G_{bc}^v\!\downarrow$) the ratio $\hat{c}_0$ is analogous to the bottlenecked situation of the b and a level. The relaxation rates $G_{bc}^v\!\uparrow$ and G_{ba}^v are then the stability determining rates for the decay of b atoms. For example, for a bubble of $V=1$ mm^3, $A/V=50$ cm^{-1}, $K_{bc}^{\text{eff}} \simeq G_{bc}^v\!\downarrow$ at 0.8 K (using the numerical values given in Table I).

Combining Eqs. (4.2) and (4.3) the number decay is given by

$$\dot{N}/(Vb^2) = -2[\zeta_0 G_{ba}^v + \eta_0 G_{bc}^v\!\uparrow] \tag{4.4}$$

with $\zeta_0 \equiv k_{ab}^{\text{eff}}/(K_{ab}^{\text{eff}} - G_{ba}^v - G_{bc}^v\!\uparrow)$ and $\eta_0 \equiv k_{bc}^{\text{eff}}/(K_{bc}^{\text{eff}} + G_{bc}^v\!\downarrow)$. The decay is thus bottlenecked by nuclear and electronic relaxation as long as $K_{bc}^{\text{eff}} \gg G_{bc}^v\!\downarrow(\eta_0 \simeq 1)$ and $K_{ab}^{\text{eff}} \gg G_{ba}^v(\zeta_0 \simeq 1)$.

When third-order effects are included in Eqs. (4.2), the rate equations become, up to first order in $\hat{a}$ and $\hat{c}$ (ignoring the small contribution of $\hat{d}$):

$$\dot{A}/(Vb^2) = -K_{ab}^{\text{eff}}\hat{a} + G_{ba}^v - K_{abb}^v b\hat{a} \ ,$$

$$\dot{B}/(Vb^2) = -K_{ab}^{\text{eff}}\hat{a} - G_{ba}^v - K_{bc}^{\text{eff}}\hat{c} - G_{ab}^v\!\uparrow(1+\hat{c}) + G_{bc}^v\!\downarrow\hat{c}$$
$$\qquad -(2+\xi)K_{bbb}^v b - K_{bbc}^v b\hat{c} - K_{abb}^v b\hat{a} \ , \tag{4.5}$$

$$\dot{C}/(Vb^2) = -K_{bc}^{\text{eff}}\hat{c} + G_{bc}^v\!\uparrow(1+\hat{c}) - G_{bc}^v\!\downarrow\hat{c}$$
$$\qquad + \xi K_{bbb}^v b - K_{bbc}^v b\hat{c} \ .$$

Summing results, we find a rate equation for N:

TABLE I. Some rate constants used in the analysis. Rate constants G_{ba}^v, G_{bc}^v, and K_{bbb}^v follow from the analysis of our data.

	Rate constants	Reference
Two-body recombination	$K_{ab}^{\text{eff}} = A/V[\lambda_{th}\exp(\varepsilon_a/k_BT)]^2 2.5 \times 10^{-8}T^{1/2}B^{-2} + K_{ab\text{He}}$ cm^3 s^{-1}	11
	$K_{aa}^{\text{eff}} = 2.2 K_{ab}^{\text{eff}}$	11
	$K_{bc}^{\text{eff}} = A/V[\lambda_{th}\exp(\varepsilon_a/k_BT)]^2 3.9 \times 10^{-5}T^{1/2} + K_{bc\text{He}}$ cm^3 s^{-1}	31 and 32
	with $E_a = 1.15$ K	
	$K_{bc\text{He}} = 2.8(3) \times 10^{-33}n_{\text{He}}$ cm^3 s^{-1}	33
	$K_{ab\text{He}} = \varepsilon^2 K_{bc\text{He}}$, $n_{\text{He}} \simeq 4.65 \times 10^{13}\exp(10.1T)$ cm^{-3}	33
Two-body relaxation	$G_{ab}^v = T^{1/2}(1+16.68/B)^2 6.9(6) \times 10^{-22}$ cm^3 s^{-1}	This work[a]
	$G_{bc}^v\!\downarrow = 12(4) \times 10^{-16}$ cm^3 s^{-1}	This work[a]
	$G_{bc}^v\!\uparrow = G_{bc}^v\!\downarrow\exp(-1.35B/T)$ cm^3 s^{-1}	This work[a]
Three-body recombination	$K_{bbb}^v = 2.0(5) \times 10^{-39}$ cm^6 s^{-1} at $B=9.8$ and 9 T	This work
	$K_{bbc}^v = 3(1) \times 10^{-33}$ cm^6 s^{-1}	This work[a] and 14
	$K_{abb}^v = \varepsilon^2 K_{bbc}^v$ cm^6 s^{-1}	This work[a] and 14

[a]We use $T^{1/2}$ behavior for G_{ba}^v near 700 mK to scale data.

$$\dot{N}/(Vb^2) = -2(K_{ab}^{\text{eff}}\hat{a} + K_{bc}^{\text{eff}}\hat{c} + K_{bbb}^v b$$

$$+ K_{abb}^v b\hat{a} + K_{bbc}^v b\hat{c}) \ . \tag{4.6}$$

Here $\hat{a}$ and $\hat{c}$ do not go to a well-defined limit value, but change as a function of density due to the presence of third-order terms in Eqs. (4.5). An estimate of the equilibrium value of $\hat{a}$ and $\hat{c}$ is found by assuming $\dot{\hat{a}}$ and $\dot{\hat{c}}$ to be small. Under the nearly isobaric conditions of our bubble measurements this is a plausible assumption. One then finds b-density-dependent ratios

$$\hat{a} = G_{ba}^v / [K_{ab}^{\text{eff}} - G_{ba}^v - G_{bc}^v \uparrow + K_{abb}^v b - (2+\xi)K_{bbb}^v b] \ , \tag{4.7}$$

$$\hat{c} = (G_{bc}^v \uparrow + \xi K_{bbb}^v b)/(K_{bc}^{\text{eff}} + G_{bc}^v \downarrow + K_{bbc}^v b) \ .$$

At low densities Eqs. (4.7) reduce to Eqs. (4.3). The influence of the three-body terms on $\hat{c}$ is substantial, even for the experimental conditions reported here: e.g., $B = 9.8$ T, $T = 0.75$ K and $b = 5 \times 10^{17}$ cm^{-3} gives $\hat{c} = 6 \times 10^{-9}$ without and $\hat{c} = 1 \times 10^{-7}$ with three-body terms. This shows that the production of c-state atoms is mainly due to three-body recombination (K_{bbb}^v) events and not to electronic relaxation ($G_{bc}^v \uparrow$). As a consequence the c-state occupation is a factor of 5 larger than one expects for thermal equilibrium ($\hat{c} \simeq 2 \times 10^{-8}$). At lower temperatures the factor may become substantially larger than 5.

Substituting Eqs. (4.7) into Eq. (4.6) and arranging the equation in order of b density gives

$$\dot{N}/(Vb^2) = -2(\zeta G_{ba}^v + \eta G_{bc}^v \uparrow)$$

$$-2[(1+\xi\eta)K_{bbb}^v + K_{abb}^v \zeta(G_{ba}^v / K_{ab}^{\text{eff}})$$

$$+ K_{bbc}^v \eta G_{bc}^v \uparrow / K_{bc}^{\text{eff}}]b$$

$$-2[(K_{bbc}^v K_{bbb}^v / K_{bc}^{\text{eff}})\xi\eta]b^2 \ , \tag{4.8}$$

with

$$\eta = K_{bc}^{\text{eff}} / (K_{bc}^{\text{eff}} + G_{bc}^v \downarrow + K_{bbc}^v b) \ ,$$

and

$$\zeta = K_{ab}^{\text{eff}} / [K_{ab}^{\text{eff}} - G_{ba}^v - G_{bc}^v \uparrow + K_{abb}^v b - (2+\xi)K_{bbb}^v b] \ .$$

Note that arranging in order of b density is not completely adequate, because η and ζ depend on the b density and also that there is a small term proportional to the fourth power of the density due to cross terms. We emphasize that this fourth-order (and higher-order) term contributes to the decay, although a four-body term is not explicitly included in the rate equations.

One would like to compare expression (4.8) with the experimentally observed C_2 and C_3 [see Eq. (3.2)]; it is virtually impossible to extract the small fourth-order term from the experiment. Good agreement with a numerical solution of the equilibrium values of $\hat{a}$, $\hat{c}$, and $\hat{d}$ from an extended equation including all rate constants is obtained by expansion of η, ζ, etc., into a density-independent part $\eta_0 = \eta(b=0)$, $\zeta_0 = \zeta(b=0)$ and a small density-dependent part

$$\eta = \eta_0 \{ 1 - [K_{bbc}^v / (K_{bc}^{\text{eff}} + G_{bc}^v \downarrow)]b$$

$$+ [K_{bbc}^v / (K_{bc}^{\text{eff}} + G_{bc}^v \downarrow)]^2 b^2 - \cdots \}$$

and

$$\zeta = \zeta_0 \{ 1 - [K_{abb}^v / (K_{ab}^{\text{eff}} - G_{ba}^v - G_{bc}^v \uparrow)]b$$

$$+ [(2+\xi)K_{bbb}^v / (K_{ab}^{\text{eff}} - G_{ba}^v - G_{bc}^v \uparrow)]b + \cdots \}$$

and using only terms up to first order in b density. This approach is valid as long as $K_{bbc}^v b \ll K_{bc}^{\text{eff}} + G_{bc}^v \downarrow$, etc. This results in

$$C_2 = 2(\zeta_0 G_{ba}^v + \eta_0 G_{bc}^v \uparrow)/(1+\hat{a}_0)^2 \ ,$$

$$C_3 = 2(\theta_b K_{bbb}^v + \theta_c K_{bbc}^v - \theta_a K_{abb}^v)/(1+\hat{a}_0)^3 \ , \tag{4.9}$$

with

$$\theta_b \equiv 1 + \xi\eta_0 + (2+\xi)\zeta_0^2(G_{ba}^v / K_{ab}^{\text{eff}}) \simeq 1 + \xi\eta_0 \ ,$$

$$\theta_c \equiv \eta_0^2(G_{bc}^v \downarrow / K_{bc}^{\text{eff}})^2 \exp(-1.35B/T) \ ,$$

$$\theta_a \equiv (1 + G_v^{bc} \uparrow / G_{ba}^v)(\zeta_0 G_{ba}^v / K_{ab}^{\text{eff}})^2 \ ,$$

and $\hat{a}_0$ defined by Eqs. (4.3).

The second-order coefficient C_2, [i.e., the linear coefficient of $F(n)$ in Eq. (3.1)], has contributions from the nuclear and electronic relaxation. The third-order coefficient C_3 consists of three terms. (a) The K_{bbb}^v term. The number of b-state atoms lost per K_{bbb}^v event is expressed by the proportionality factor, $2\theta_b$, in front of the K_{bbb}^v coefficient. In the limit that $\eta_0 \rightarrow 1$ and $\zeta_0 \rightarrow 1$ (i.e., K_{bc}^{eff} and K_{ab}^{eff} dominating), the effective loss increases to $2\theta_b = 2(1+\xi) = 3.82$ b atoms per K_{bbb}^v event. Physically this means that in one K_{bbb}^v event, two atoms are lost directly and 2ξ atoms are lost by the third body flipping to the c state followed by K_{bc}^{eff} recombination. (b) The K_{bbc}^v term arises from the population of the c level.[30] The θ_c is orders of magnitude smaller than θ_b. However, it has to be taken into account since K_{bbc}^v is much larger than K_{bbb}^v. (c) Likewise the K_{abb}^v term arises from population of the a level. One might wonder why a minus sign appears in front of the K_{abb}^v term in Eqs. (4.9). However, this sign follows quite logically from Eq. (4.6). It originates in the influence of K_{abb}^v on the polarization [Eqs. (4.7)]. Increase of K_{abb}^v decreases $\hat{a}$, with the overall result that the negative third-order contribution (third order in b) of the $K_{ab}^{\text{eff}}\hat{a}$ term slightly overcompensates the positive third-order contribution of the $K_{abb}^v b\hat{a}$ term. At this point it is also useful to note that in the doubly-polarized gas even a dramatic increase in K_{abb}^v does not lead to a significant increase in recombination. The recombination rate is dominated by the relaxation processes (G_{ba}^v) and (G_{bc}^v) and the dipolar mechanism (K_{bbb}^v).

The analysis as presented above is only valid for a doubly-polarized gas ($\hat{a} \ll 1$) and thus one would like to have a good estimate of $\hat{a}$ to check the applicability of Eqs. (4.1)—(4.9). As follows from Eq. (4.7), $\hat{a}$ depends on the ratio of G_{ba}^v and K_{ab}^{eff}. Measurements of K_{ab}^{eff} are available up to 500 mK.[31-33,10,11,13] To obtain K_{ab}^{eff} at the temperatures used in this experiment (~ 700 mK) one has to extrapolate from low temperature. Although the observed K_{ab}^{eff} in the as yet experimentally accessed temperature range give agreement between the different authors within a factor of 2, extrapolation of these measurements gives differences as large as a factor of 4. To allow analysis of our data we choose a typical value (see Table I)

$K_{ab}^s B^2 T^{-1/2} = 2.5 \times 10^{-8}$ cm^{2}s^{-1} (with $\varepsilon_a = 1.15$ K).[34]
Using these values leads to a rather poor double polarization ($\hat{a} \simeq 0.15$) and thus Eqs. (4.5) cannot be used for a rigorous analysis of our experiment. One has to include contributions from processes involving two or more a-state atoms [e.g., $K_{aa}^s \simeq 2.2 K_{ab}^s$ (Refs. 11, 35, and 13), K_{aab}^v, K_{aaa}^v and processes of combinations of a-state atoms with c- and d-state atoms] and solve this extended form of Eqs. (4.1) numerically to obtain the density-dependent equilibrium values for $\hat{a}$, $\hat{c}$, and $\hat{d}$ and the resulting rate $\dot{N}/n^2$. C_2 and C_3 are then determined from fits to the calculated overall rates as a function of n. Such a procedure does not allow explicit differentiation between contributions of the different processes (K_{bbb}^v, K_{abb}^v, etc.). However, qualitatively the linearized expressions (4.1)–(4.9) are still valid and can guide the understanding of the system.

As an illustration we show in Fig. 10 the full numerical solution (dashed-dotted line, based on Table I) and one based on a second-order fit to the data (dashed line). It is impossible to discriminate between these two approaches within experimental accuracy. The dotted line in Fig. 10 is the numerical solution for a volume of $V_0 = 0.02$ mm^3 ($A/V = 150$ cm^{-1}). This illustrates the influence of the A/V ratio on the decay. As follows from Fig. 8 the A/V ratio increases for smaller bubbles and subsequently K_{ab}^{eff} and K_{bc}^{eff} increase, resulting in a larger C_2 and C_3 [see Eqs. (4.9)].

Using the approach of Eqs. (4.9), one can interpret the data presented in Sec. IV B. The results for the field dependence of C_2 [Fig. 14(a)] give for high fields, where $G_{bc}^v \uparrow$ is suppressed, a bulk nuclear relaxation constant corresponding to $G_{ba}^v (1 + 16.68/B)^{-2} = 6.9(9) \times 10^{-22}$ cm^3 s^{-1} at 710 mK [dashed line in Fig. 14(a)]. This is in agreement with the previous lower temperature measurements[10-12] and theory.[36-38] The error in G_{ba}^v includes a systematic error in the reference height as measured by the level gauge of about 0.3 mm helium. Note that the dashed line does not simply scale according to $(1 + 16.68/b)^2$. Such a relationship is only to be expected if the contribution of the K_{aa}^{eff} term is negligible and the equilibrium value of $\hat{a}$ is independent of magnetic field. In our measurements we estimate a $\simeq 30\%$ of K_{aa}^{eff} relative to K_{ab}^{eff}, while $\hat{a}$ varies from $\hat{a} = 0.17$ for $B = 6$ T to $\hat{a} = 0.21$ for $B = 10$ T. The dashed lines are given by the expression

$$(2\hat{a}_0 K_{ab}^{\text{eff}} + 2\hat{a}_0^2 K_a^{\text{eff}})/(1 + \hat{a}_0)^2 ,$$

note that

$$2\hat{a}_0 K_{ab}^{\text{eff}}/(1 + \hat{a}_0)^2 \simeq 2\zeta_0 G_{ba}^v .$$

For low fields an/or high temperatures ($B/T < 10$ T/K) the contribution of the electron-spin relaxation, $2\eta_0 G_{bc}^v \uparrow$, becomes important. This is shown in Fig. 14(a) as a deviation from the dashed line. The full line in this figure shows the sum of both contributions with a best value

$$G_{bc}^v \uparrow = 12(4) \times 10^{-16} \exp(-1.35 B/T) \text{ cm}^3 \text{s}^{-1} ,$$

in agreement with the calculation of Lagendijk et al.[36]

$$G_{bc}^v \uparrow = 9.7 \times 10^{-16} \exp(-1.35 B/T) \text{ cm}^3 \text{s}^{-1} .$$

This value is also in good agreement with the value of Bell et al.,[14]

$$\eta_0 G_{bc}^v \downarrow = 10(1) \times 10^{-16} \text{ cm}^3 \text{s}^{-1} ,$$

when using $\eta_0 = 0.85(8)$, a typical value for the M.I.T. geometry. The exponential character of $G_{bc}^v \uparrow = G_{bc}^v \downarrow \exp(-1.35 B/T)$ is illustrated in Fig. 16, where

$$C_2 - (2\hat{a}_0 k_{ab}^{\text{eff}} + 2\hat{a}_0^2 K_{aa}^{\text{eff}})/(1 + \hat{a}_0)^2 \simeq 2\eta_0 G_{bc}^v \uparrow$$

is plotted versus B/T. This corresponds to the deviation from the dashed line in Fig. 14(a). The dotted line in Fig. 16 is based on the theoretical value of Lagendijk et al. About 30% of the difference between the dotted line and the data points can be explained by an additional contribution to C_2 from b,d recombination.

Our measurements of C_3 [Fig. 14(b)] are most reliable for high fields. For $B \geq 9$ T, $C_3 \simeq 2\theta_b K_{bbb}^v = 7(2) \times 10^{-39}$ cm^{6}s^{-1}. Excluding any explicit field dependence of K_{bbb}^v and taking into account a small correction due to θ_c and θ_a we find $k_{bbb}^v = 2.0(5) \times 10^{-39}$ cm^{6}s^{-1} and $2\theta_b = 3.27$. For low magnetic fields C_3 increases due to the contribution of the K_{bbc}^v term in Eqs. (4.9). The solid line in Fig. 14(b) is calculated with a value of $K_{bbc}^v = 3(1) \times 10^{-33}$ cm^{6}s^{-1} (see Table I), derived from the value of Bell et al.[30,15] Hardy et al.[16] found $K_{HH^4He} = 2.8(3) \times 10^{-33}$ cm^{6}s^{-1} and $K_{HH^3He} = 1.2 \times 10^{-33}$ cm^{6}s^{-1} for bulk recombination rates in $B = 0$. The systematic errors in pressure p do not permit a useful fit for K_{bc} from our data points. However, the measured value of C_3 seems to be systematically higher than the calculated one. Choosing a substantially larger value for K_{bbc}^v increases C_3 at low fields, but not sufficient to obtain a fit for the third-order rate at 6 and 7 T. For example, increasing K_{bbc}^v by a factor of 10 increases C_3 only by $\simeq 15\%$. This problem was checked extensively both by numerical solution of the extended form of Eqs. (4.9) and by direct calculation of
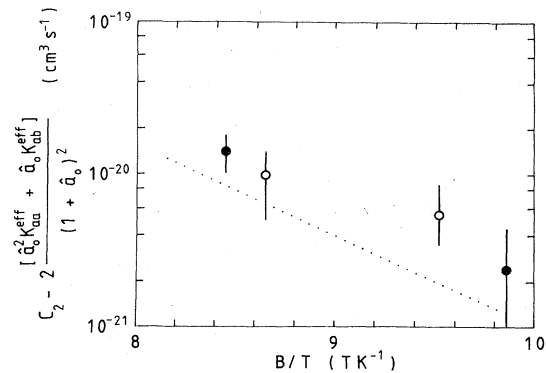

FIG. 16. Exponential dependence of the $G_{bc}^v \uparrow$ contribution to C_2 on B/T (see text). The dotted line is the calculated relaxation by Lagendijk et al. (Ref. 36) (see text). Solid circles are data points at different field and $T = 710$ mK. Open circles are at $B = 8$ T and different temperatures.

the decay curves, both in the isobaric and isochoric case. The problem originates from the change of the c population due to K^v_{bbc} recombination [see Eq. (4.7)] and the subsequent influence on $\eta G^v_{bc}\uparrow$. The calculation of the decay show that $\hat{a}$ and $\hat{c}$ remain close to the density-dependent equilibrium values, even if the starting conditions are different. For densities between 10^{17}–10^{18} atoms /cm^{-3} this equilibrium is achieved under isobaric conditions within 20 s, much faster than the time used for precompression of the gas (see Sec. II B).

Our results for the bulk three-body recombination rates are best compared to the measurements of Bell et al.[14,8] at 600 mK between 4 and 8 T. These authors find a K^v_{bbc} contribution[30] for the three-body rate at low field that is suppressed exponentially for increasing field and a contribution of K^v_{bbb} that slightly decreases for increasing magnetic field. This is in contradiction with theory for K^v_{bbb} (Refs. 28 and 29) [dotted line in Fig. 14(b)] showing a rate increasing with field. At 600 mK, Bell et al.[14,8] found $2\theta_b K^v_{bbb} = 7.9(4) \times 10^{-39}$ cm^6 s^{-1} from a fit to the field dependence between 4 and 8 T. For their conditions $2\theta_b = 3.7$, which implies $K^v_{bbb} = 2.1(1) \times 10^{-39}$ cm^6 s^{-1}, in good agreement with our results.

The field dependence of the three-body term is of importance to decide if the stability of the gas is increased by going to higher fields than used up to now ($B < 11$ T). We cannot reliably separate the K^v_{bbb} contribution from other three-body contributions to the field dependence of C_3. As long as $\hat{a} < 1\%$, one can apply the set of Eqs. (4.1) and the subsequent analysis resulting in Eqs. (4.9). At high fields the contributions due to thermal population of the c state are suppressed, leaving only the K^v_{ab} and K^v_{bbb} contributions to C_3. The denominator $1 + \hat{a}_0$ in Eqs. (4.9) increases as a function of magnetic field due to the intrinsic field dependence of G^v_{ba} and K^{eff}_{ab}. Thus $2\theta_b / (1 + \hat{a}_0)^3$ decreases, resulting in a decreasing C_3 if K^v_{bbb} were constant. However, one has to take into account the K^v_{abb} term as well since $\hat{a}_0 \neq 0$, resulting in a complicated overall field dependence of C_3 which is a function of the intrinsic field dependence of K^v_{bbb} and K^v_{abb}. As mentioned, the dipolar K^v_{bbb} rate constant is predicted to increase by a factor of 2 for $B = 6$ to 10 T.[28,39] The exchange recombination rate K^v_{abb} is presumably proportional to ε^2 ($\varepsilon = a / 4\mu_B B$ the hyperfine mixing parameter, $K^v_{abb} \simeq \varepsilon^2 K^v_{bbc}$). According to Kagan et al.[28] at $T = 0$ K the K^v_{abb} exchange recombination vanishes due to quantum interference. At finite temperatures, where the experiments are done, the K^v_{abb} exchange rate does not vanish and may contribute to C_3. However, setting $K^v_{bbb} = 0$ and using $K^v_{abb} = \varepsilon^2 K^v_{bbc}$ underestimates the measured C_3 at the high fields, indicating that K^v_{bbb} cannot be ignored.

D. Thermal equilibrium

The major concern in the analysis is the thermal equilibrium of the gas; the gas should have the same temperature as the body of the cell and liquid helium, and should have a uniform internal temperature distribution. Let us discuss the possibility that the deviation of the decay rate from two-body behavior at high density, which we attri-

bute to three-body effects, could be explained by heating of the gas and two-body effects. In particular, at 9.8 T, 750 mK we would have to explain that the rate $\tau^{-1} = 14 \times 10^{-3}$ s^{-1} at $n = 10^{18}$ cm^{-3} is about a factor of 2 larger than expected from two-body relaxation G^v_{ba}. Only above 950 mK the $G^v_{bc}\uparrow$ contribution to the relaxation would make the relaxation sufficiently fast to account for this effect. However, this implies a temperature gradient of 200 mK.

There are three stages in the thermal conduction of the recombination heat to the body of the cell that can be bottlenecking, thus causing a difference between measured body temperature and the gas temperature. The first source for a gradient is the finite heat conductivity of the H↓↑ gas ($\kappa = 3.5 \times 10^{-3}$ W/K m)[40] at these densities. For a gas of $n = 10^{18}$ cm^{-3}, the mean free path $\lambda = 3\kappa / (nC_v \bar{v}) \simeq 4$ μm at 700 mK, a factor 250 smaller than the typical bubble diameter (1 mm), allowing us to treat the conductivity problem in the hydrodynamic regime:[26] $\nabla \kappa \nabla T = -q$, where q is the (local) heat production per unit volume per unit time. The recombination heat is produced by atoms recombining on the wall. (K^{eff}_{bc}) or, if we include three-body effects, in the bulk [K^v_{bbb} and K^v_{bbc} term in Eqs. (4.9)]. The energy transfer between the highly excited molecule produced in the recombination reaction and the H↓↑ gas is not known in detail. Assume for simplicity that half of the produced recombination energy is transferred in such a way that q is uniform over the sample. In the limit of small gradients, the average temperature variation, $\langle \Delta T \rangle = (1/V) \int_V (T - T_0) dV$, where T_0 is the surface temperature, is then easily estimated, noting that κ is essentially temperature independent[40] and using $q = (\frac{1}{2}) D dN / dt = (\frac{1}{2}) Dn\tau^{-1}$, where $D = 7.2 \times 10^{-19}$ J is the dissociation energy of H$_2$. For a 1-mm^3 spherical bubble (radius $R = 0.6$ mm) at 9.8 T, $\tau^{-1} = 14 \times 10^{-3}$ s^{-1} and $n = 10^{18}$ cm^{-3}, we find $q = 5$ μW mm^{-3} and $\langle \Delta T \rangle = (\frac{1}{15}) qR^2 / \kappa = 30$ mK. Although this is substantial, it is not sufficient to explain the deviation from two-body behavior, because G^v_{ba} is only weakly dependent on temperature and the field is still sufficiently high to suppress electron-spin relaxation $G^v_{bc}\uparrow$. For the true bubble shape (Fig. 8) the larger A/V ratio and the flat geometry of the bubble will lower $\langle \Delta T \rangle$. To describe the situation in the gas for larger temperature gradients, including the three-body effects, one has to use a temperature and density-dependent function for q. Kagan et al.[26] investigated this problem for a plane geometry by assuming either strictly local or global heat production (i.e., averaged over the temperature-density distribution). In both cases there is a critical density (n_c) depending on the distance (L) between the planes, above which there is not a stable solution to the problem ($n_c \simeq 2 \times 10^{18}$ cm^{-3} for $L = 1$ mm). The main source of this instability is the K^v_{bbc} term that depends on $G^v_{bc}\uparrow$ and thus increases exponentially with temperature.

The second stage in the heat conduction that can cause temperature gradients is the thermal boundary resistance (Kapitza resistance) between the H↓↑ gas and the liquid helium. Using simple gas-kinetic arguments, one can estimate the heat transfer across a helium surface:

$\dot{Q} = \frac{1}{4}n\bar{v}A\alpha(T)\Delta E$, where $\bar{v} = (8k_B T/\pi m)^{1/2}$ is the average thermal velocity, A is the helium surface area, $\alpha(T)$ is the energy accommodation coefficient, and $\Delta E = 2k_B \Delta T$ is a measure for the energy transfer during a collision with the wall. Using $\alpha(T) = 0.2$ from Salonen et al.,[41] one finds $\Delta T = 4$ mK in a spherical bubble of 1 mm^3 at 9.8 T and $n = 10^{18}$ cm^{-3}, again too small to explain the deviations from two-body behavior.

The final stage in the heat conduction is the heat transport through the ^{4}He liquid ($\kappa = 100$ W/K m for pure ^{4}He at 700 mK)[42] and the thermal boundary resistance between helium and the silver sinter. For pure ^{4}He in our geometry the typically $\dot{Q} < 5$ μW recombination heat can easily be conducted and coupled to the 1-m^2 silver sinter surface. For ^{3}He-^{4}He mixtures, the heat conductivity decreases as a function of the ^{3}He concentration rather drastically (at 300 mK, $\kappa = 15$ W/K m for pure ^{4}He and $\kappa = 0.2$ W/K m for 1.3% ^{3}He in ^{4}He).[42] This may explain the irreproducibility and thermal problems we had with our measurements on mixtures.

V. CONCLUSIONS

In this paper a new experimental technique based on volume compression up to 5 orders of magnitude and observation of the volume decay under quasi-isobaric conditions was used to study H↓↑ at high densities. The main difference between this technique and the usual isochoric technique is the possibility to study a small sample of gas at high density (up to 2×10^{18} cm^{-3}) for a period of minutes. In addition to the column head of helium used to apply the pressure on the gas, surface tension increases the total gas pressure. This surface tension can be accounted for by a simple model for the bubble shape.

With this technique we identified the two-body electronic relaxation rate $G_{bc}^v \downarrow = G_{bc}^v \uparrow \exp(1.35 B/T) = 12(4)$

$\times 10^{-15}$ cm^{3}s^{-1} at $T = 710$ mK, a thermally activated process that becomes noticeable at high temperature and/or low fields ($B/T \leq 10$ T/K). At high densities dipolar recombination becomes an important destabilization process; $K_{bbb}^v = 2.0(5) \times 10^{-39}$ cm^{6}s^{-1} at 9.8 T and 750 mK. Also for three-body rates the thermal population of the c level becomes observable at $B/T \leq 10$ T/K. The magnetic field dependence of the three-body process, especially interesting at high fields, is not clear from our measurements; more data at higher fields are required. An additional complication is the degree of double polarization in the gas, leading to a contribution from K_{abb}^v to the three-body rate. At high densities the gas appears to be susceptible to explosions, especially in large bubbles.

The new technique has good prospects in increasing the maximum density obtainable in the gas by going to very small bubbles and thus reducing the problems of out-of-thermal equilibrium in the gas.

Note added. After submission of our manuscript we received a copy of an extensive paper by Bell et al.[8] which gives a detailed account of the experiments done at the Massachusetts Institute of Technology. In view of the importance of this paper, we have added some references to this work in the present text.

ACKNOWLEDGMENTS

[1]I. F. Silvera, Physica 109&110B, 1499 (1982).

[2]J. T. M. Walraven, in Proceedings of the International Conference of Low-Temperature Physics, LT-17, edited by U. Eckern, A. Schmid, W. Weber, and H. Wühl [Physica 126B+C, 176 (1984)].

[3]T. J. Greytak and D. Kleppner, in New Trends in Atomic Physics, edited by G. Grynberg and R. Stora (North-Holland, Amsterdam, 1984), Vol. II, p. 1125.

[4]T. D. Lee, K. Huang, and C. N. Yang, Phys. Rev. 106, 1135 (1957).

[5]R. Sprik, J. T. M. Walraven, and I. F. Silvera, Phys. Rev. Lett. 51, 479 (1983); 51, 942(E) (1983).

[6]H. F. Hess, D. A. Bell, G. P. Kochanski, R. W. Cline, D. Kleppner, and T. J. Greytak, Phys. Rev. Lett. 51, 483 (1983).

[7]H. F. Hess, D. A. Bell, G. P. Kochanski, D. Kleppner, and T. J. Greytak, Phys. Rev. Lett. 52, 1520 (1984).

[8]D. A. Bell, H. F. Hess, G. P. Kochanski, S. Buchman, L. Pollack, Y. M. Xiao, D. Kleppner, and T. J. Greytak, Phys. Rev. B (to be published).

[9]B. W. Statt and A. J. Berlinsky, Phys. Rev. Lett. 45, 2105 (1980).

[10]R. W. Cline, T. J. Greytak, and D. Kleppner, Phys. Rev. Lett.

47, 1195 (1981).

[11]R. Sprik, J. T. M. Walraven, G. H. van Yperen, and I. F. Silvera, Phys. Rev. Lett. 49, 153 (1982).

[12]B. Yurke, J. S. Denker, B. R. Johnson, N. Bigelow, L. P. Levy, D. M. Lee, and J. H. Freed, Phys. Rev. Lett. 50, 1137 (1983).

[13]B. W. Statt, A. J. Berlinsky, and W. N. Hardy, in Proceedings of the International Conference on Low-Temperature Physics, LT-17, Ref. 2, p. 467; Phys. Rev. B 31, 3169 (1985); M. W. Reynolds, I. Shinkoda, W. N. Hardy, A. J. Berlinsky, F. Bridges, and B. W. Statt, Phys. Rev. B 31, 7503 (1985).

[14]D. A. Bell, G. P. Kochanski, L. Pollack, H. F. Hess, D. Kleppner, and T. J. Greytak, in Proceedings of the International Conference on Low-Temperature Physics, LT-17, Ref. 2, p. 449.

[15]D. A. Bell, G. P. Kochanski, D. Kleppner, and T. J. Greytak, in Proceedings of the International Conference on Low-Temperature Physics, LT-17, Ref. 2, p. 541.

[16]W. N. Hardy, M. Morrow, R. Jochemsen, and A. J. Berlinsky, Physica 109&110B, 1964 (1982).

[17]J. T. M. Walraven and I. F. Silvera, Phys. Rev. Lett. 44, 168 (1980).

[18]J. T. M. Walraven and I. F. Silvera, Rev. Sci. Instrum. **53**, 1167 (1982).

[19]The relative dielectric constant ϵ_r is obtained by using the Clausius-Mossotti relation $(\epsilon_r-1)/(\epsilon_r-2)=np/3\epsilon_0$, where $p/(4\pi\epsilon_0)=0.2044\times10^{-24}$ cm^3 the polarizability for ^{4}He [C. E. Chase, E. Maxwell, and W. E. Millet, Physica **27**, 1129 (1961)], and $n=2.182\times10^{22}$ cm^{-3} the density of ^{4}He below 1 K [E. C. Kerr and R. P. Taylor, Ann. Phys. **26**, 292 (1964)].

[20]I. F. Silvera and J. T. M. Walraven, Phys. Rev. Lett. **44**, 164 (1980).

[21]C. T. van Degrift, Rev. Sci. Instrum. **46**, 599 (1975).

[22]W. J. Duffin, *Electricity and Magnetism* (McGraw-Hill, New York, 1965).

[23]*Handbook of Chemistry and Physics*, edited by R. C. Weast (Chemical Rubber, Cleveland, 1971).

[24]A. W. Adamson, *Physical Chemistry of Surfaces* (Wiley, New York, 1976).

[25]J. R. Eckardt, D. O. Edwards, S. Y. Shen, and F. M Gasparini, Phys. Rev. B **16**, 1944 (1977).

[26]Yu. Kagan, G. V. Shlyapnikov, and I. A. Vartanyantz, Phys. Lett. **101A**, 27 (1984).

[27]T. Tommila, S. Jaakkola, M. Krusius, K. Salonen, and E. Tjukanov, *Proceedings of the International Conference on Low-Temperature Physics, LT-17*, Ref. 2, p. 453.

[28]Yu. Kagan, I. A. Vartanyantz, and G. V. Shlyapnikov, Zh. Eksp. Teor. Fiz. **81**, 1113, (1981) [Sov. Phys.—JETP **54**, 590 (1982)].

[29]Note that Bell *et al.* (Ref. 15) extracted $\xi=0.93$ for $B=10$ T from Kagan *et al.* (Ref. 28). We use the value $\xi=0.91$, which was obtained by de Goeij and Verhaar and checked to be independent of magnetic field within the range of experimental interest [$5<B<10$ T; B. J. Verhaar (private communication)].

[30]Note that our expression for the K_{bbc}^v contribution to C_3 is proportional with $(G_{bc}^v \downarrow /K_{bc}^{\text{eff}})$ (Ref. 2) in contrast to the expression used by Bell *et al.* (Ref. 15).

[31]A. P. M. Matthey, J. T. M. Walraven, and I. F. Silvera, Phys. Rev. Lett. **46**, 668 (1981).

[32]A. P. M. Matthey (unpublished).

[33]M. Morrow, R. Jochemsen, A. J. Berlinsky, and W. N. Hardy, Phys. Rev. Lett. **46**, 195 (1981); **47**, 455 (1981).

[34]The values for K_{ab}^s and ε_a are strongly coupled. Our particular choice gives a reasonable fit for K_{ab}^{eff} in the experimentally accessed regime (Refs. 31–33, 10, and 12).

[35]G. H. van Yperen, I. F. Silvera, J. T. M. Walraven, J. Berkhout, and J. G. Brisson, Phys. Rev. Lett. **50**, 53 (1983); G. H. van Yperen, J. T. M. Walraven, and I. F. Silvera, Phys. Rev. B **30**, 2386 (1984).

[36]A. Lagendijk, G. H. van Yperen, and J. T. M. Walraven, J. Phys. (Paris) Lett. **45**, L929 (1984).

[37]R. M. C. Ahn, J.P.H.W. v. d. Eynde, and B. J. Verhaar, Phys. Rev. B **27**, 5424 (1983).

[38]E. D. Siggia and A. E. Ruckenstein, Phys. Rev. B **23**, 3580 (1981).

[39]L. P. H. de Goeij, J. P. J. Driessen, B. J. Verhaar, and J. T. M. Walraven, Phys. Rev. Lett. **53**, 1919 (1984).

[40]C. Lhuillier, J. Phys. **44**, 1 (1983).

[41]K. Salonen, S. Jaakkola, M. Karhunen, E. Tjukanov, and T. Tommila, in *Proceedings of the International Conference on Low-Temperature Physics, LT-17*, Ref. 2, p. 543; K. T. Salonen, I. F. Silvera, J. T. M. Walraven, and G. H. van Yperen, Phys. Rev. B **25**, 6002 (1982).

[42]R. L. Rosenbaum, J. Landau, and Y. Eckstein, J. Low Temp. Phys. **16**, 131 (1974).